Charged Higgs Bosons at the LHC under the Type II 2HDM.

Víctor Rodríguez Lorenzo[1,2]
E-mail: vrl209@alumnos.unican.es

[1] *Department of Physics and Technology, University of Bergen, Bergen, Norway*
[2] *Faculty of Sciences, University of Cantabria, Cantabria, Spain*

1st December 2022

Abstract

The production process of a charged Higgs boson H^+, and its almost instantaneous decay to a tau τ^+ and tau neutrino ν_τ, have been studied for a head-on collision between protons at the LHC, using its characteristic Parton Distribution Function (PDF) to identify the most likely quarks that interact in the process. Following that, the analysis of the conservation laws for the resultant decay has enabled to deduct the angular distributions for the momenta of the final leptons (polar angle θ and azimuthal angle ϕ), while the application of Lorentz transformations has made it possible to examine these magnitudes for both the laboratory and the charged Higgs rest frame. Eventually, this has lead to the study of a provided Les Houches Events file, to verify the predictions stated before, and later generate an own process with the use of the program *MadGraph*, obtaining the cross sections and branching ratios of different processes in the end.

KEYWORDS: Higgs Boson physics, 2 Higgs-Doublet Model, Charged Higgs, Proton-proton collisions, Beyond the Standard Model, Events generation

Contents

1 Introduction

The observation of a resonance at the Large Hadron Collider (LHC) in 2012 [1, 2], with a mass close to 125 GeV/c^2, apparently compatible with the existence of the Higgs Boson, raised the question of whether it constituted the single elementary particle predicted by the Standard Model (SM), or if it was attached to any other extended model. The so-called two Higgs-doublet model (2HDM) [3, 4] is one of the most consistent models that take the particle physics beyond the Standard Model, introducing two Higgs doublets in contrast to just one, as accepted by the SM. It is worth mentioning that there have been proposed other models consisting of three [5] or more Higgs doublets, which will not be considered.

This extension of the SM, therefore, considers a 'family' of five physical scalar Higgs bosons (with the two complex scalar doublets considered, eight fields can be created, three of these being "eaten" by the $W^{\pm}$ and Z^0 gauge bosons), which are characterized by different masses and charges: the CP even neutral Higgs bosons h and H(with $m_H > m_h$ by convention), a CP odd particle A and two charged Higgs bosons $H^{\pm}$.
Furthermore, depending on which type of fermions couple to which doublet, different types of classes exist for this model: Type I, where charged fermions only couple to second doublet; Type II, in which down-type quarks and charged leptons couple to one Higgs doublet, and the other to up-type quarks (which will be the one considered in this project); X, which is a lepton-specific interpretation of the model, etc.
The main purpose of this article is to analyse the production of these new particles at the LHC, and more accurately the charged Higgs pair $H^{\pm}$, studying its production processes and possible decays from a relativistic perspective.

2 Background

This project takes an approach to the production of a charged Higgs boson H, with no additional particles taking part in the process, as a consequence of the head collision between proton beams with and energy of $E = 6.5$ TeV each. The resultant H^+ is stated to have a mass of $M = 200$ GeV/c^2, eventually decaying to a charged tau τ and a tauon neutrino ν_τ.

2.1 Two Higgs Doublet Models

This particle, as mentioned before, is explained under the framework of the 2HDM, which assumes the existence of two Higgs doublets[3]:

$$\Phi_1 = \begin{pmatrix} \phi_1^+ \\ \phi_1^0 \end{pmatrix} \quad \Phi_2 = \begin{pmatrix} \phi_2^+ \\ \phi_2^0 \end{pmatrix} \tag{1}$$

For this two doublets Φ_1 and Φ_2 , the scalar potential generated has 14 parameters, and can be expressed as displayed in eq. (2).

$$\begin{aligned} V(\Phi_1,\Phi_2) = m_{11}^2\Phi_1^+\Phi_1 + m_{22}^2\Phi_2^+\Phi_2 - m_{12}^2(\Phi_1^+\Phi_2 - \Phi_2^+\Phi_1) \\ +\tfrac{\lambda_1}{2}(\Phi_1^+\Phi_1)^2 + \tfrac{\lambda_2}{2}(\Phi_2^+\Phi_2)^2 + \lambda_3\Phi_1^+\Phi_1\Phi_2^+\Phi_2 \\ +\lambda_4\Phi_1^+\Phi_1\Phi_2^+\Phi_2 + \tfrac{\lambda_5}{2}[(\Phi_1^+\Phi_2)^2 + (\Phi_2^+\Phi_1)^2] \end{aligned} \tag{2}$$

where m_{ij}^2 and λ_x are real parameters.

Similarly to the case of the Higgs boson in the Standard Model, a non-trivial value for the vacuum expectation value is obtained for each of the doublets via the minimization of the potential:

$$< \Phi_1 >= \frac{v_1}{\sqrt{2}} \qquad < \Phi_2 >= \frac{v_2}{\sqrt{2}} \tag{3}$$

Since this is not optimal, the Higgs field can be redefined so that only one doublet develops vacuum expectation value, carrying out the linear combination of eq. (4).

$$\begin{aligned} \Phi_1' &= \cos\beta\Phi_1 + \sin\beta\Phi_2 \\ \Phi_2' &= -\sin\beta\Phi_1 + \cos\beta\Phi_2 \end{aligned} \tag{4}$$

having taken into account that:

$$\tan\beta = \frac{v_2}{v_1} \tag{5}$$

This yields the following vacuum expectation values:

$$< \Phi_1' >= \frac{v}{\sqrt{2}} \qquad < \Phi_2' >= 0 \tag{6}$$

where $v = \sqrt{v_1^2 + v_2^2}$=246 GeV (the vacuum expectation value of the Higgs boson in the SM).

Considering these parametrizations, it is convenient to study now the Yukawa couplings between the Higgs bosons and the different particles [6], which results in eq. (7).

$$\mathcal{L}_{yuk} = -\sum_{f=u,d,l}\left(\frac{m_f}{v}\xi_h^f\bar{f}fh + \frac{m_f}{v}\xi_H^f\bar{f}fH - i\frac{m_f}{v}\xi_A^f\bar{f}\gamma_5 fA\right)$$

$$-\left[\frac{\sqrt{2}V_{ud}}{v}\bar{u}(m_u\xi_A^u P_L + m_d\xi_A^d P_R)dH^+\right.$$

$$\left.+\frac{\sqrt{2}m_l\xi_A^l}{v}\bar{\nu_L}l_R H^+ + h.c.\right] \quad (7)$$

in which m_f corresponds to the mass of the f fermion, γ_5 the gamma-5 matrix, V_{ud} the CKM matrix element involving the u-type u (up, charm and top) and d-type d (down, strange and bottonm) quarks, l the corresponding lepton, and P_L and P_R the left and right projection operators, respectively.
With respect to the ξ parameters, they have different values depending on with type of model is considered (Type I, Type II, Type X, etc.), corresponding to the ones organised in Table 1 (only the ones relevant to the charged Higgs are shown).

	Type I	Type II	Type X
ξ_A^u	$\cot\beta$	$\cot\beta$	$\cot\beta$
ξ_A^d	$-\cot\beta$	$\tan\beta$	$-\cot\beta$
ξ_A^l	$-\cot\beta$	$\tan\beta$	$\tan\beta$

Table 1: Yukawa couplings for the u-type quarks u, d-type quarks d and leptons l to the charged Higgs H^+.

Knowing the relations derived from these parameters, one can predict what is the main decay for the charged Higgs H^+ by simply looking at its Yukawa couplings: for a mass lower than the top quark m_t, the main channel will be one involving the biggest lepton (one anti-tau τ^+, with a tau neutrino ν_τ to verify conservation of leptonic numbers) whereas for a mass higher than the top m_t, the decay to a top t and anti-bottom$\bar{b}$ quarks will become dominant, given its enormous masses compared to the rest of the quarks, which is translated into stronger couplings.

2.2 Production processes

Attending to the explained information on the interaction, the production of the Higgs boson could be mediated by different types of processes [7], like the ones shown below:

1. The most important one for this project, and the one it will focus on, is the particle annihilation between the quarks of each of the protons involved in the collision. In the mentioned annihilation, a quark corresponding to one of the protons interacts with an antiquark of the other one (which is formed in the quark sea, where virtual $q\bar{q}$ pairs are in constant creations and annihilation), verifying the following Feynman diagrams of Figures 1, 2 and 3:

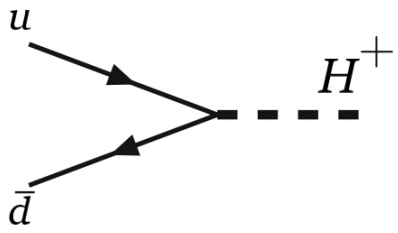

Figure 1: Feynman diagram for the annihilation process of a quark u and antiquark $\bar{d}$ into a charged Higgs H^+.

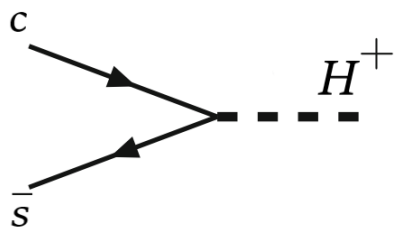

Figure 2: Feynman diagram for the annihilation process of a quark c and antiquark $\bar{s}$ into a charged Higgs H^+.

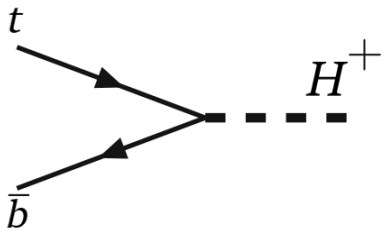

Figure 3: Feynman diagram for the annihilation process of a quark t and antiquark $\bar{b}$ into a charged Higgs H^+.

This is a direct consequence of the conservation of charge during the process: since the charge of the charged Higgs is $Q_{H^+} = 1$, a positive charged quark (namely, u, c, t with $Q = 2/3$) has to combine with a negative charged antiquark($\bar{d}$, $\bar{s}$, $\bar{b}$, with $Q = 1/3$) so that the charge is conserved in the process. Therefore, in this type of process, particles (or antiparticles) would annihilate to directly produce an H^+, with no additional particles being created. From the three generations, it is worth noting that the most likely fundamental interaction should be:

$$u\bar{d} \rightarrow H^+ \tag{8}$$

This follows from the analysis of the parton distribution function (PDF) [8] of the proton (Fig. 4), which encode the binding of the quarks and gluons inside the proton. This type of plots are essentially statistical distributions of the scattering interactions between a particle with the proton, giving the probability density of finding an specific particle with a given fraction of the momentum of the proton $xf(x)$ as a function of the Bjorken scaling factor x, which accounts for the fraction of the proton momentum that the parton has, where it can be observed that the distribution function for the u and d, from the I generation, is always higher than the distributions for the other generations, and therefore their probability to interact is also considerably higher.

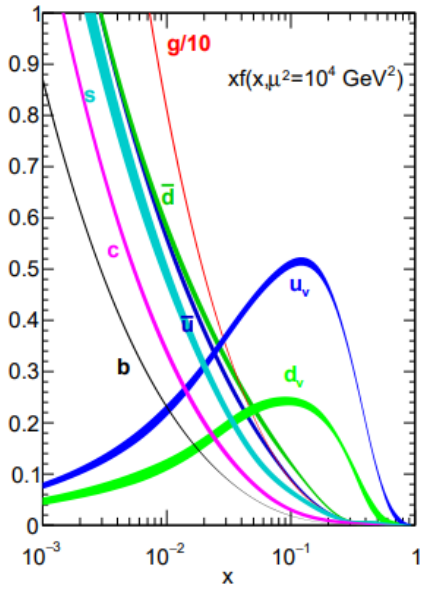

Figure 4: Parton distribution function (PDF) of the proton (taken from Ref.[9])

In Figure 4, it can also be appreciated, as expected, that the function of valence u quarks is two times the height of the valence d quarks, verifying what is expected for the structure of the proton (which contains two u quarks and one d quark). Moreover, there is no function for the t quark, since the mass for this particle is noticeably higher than the one of the proton itself (remember that the mass of the proton is approximately $m_p = 1$ GeV/c^2, whereas the top quark has a mass of $m_t = 173.34 \pm 0.27(\text{stat}) \pm 0.71(\text{syst})$ GeV/c^2)[10], making it impossible for the t quarks to exist inside the proton. This is also the reason why the function for the b quarks is the lowest among all of them, as its mass is around 4 times the mass of the proton, making it relatively unlikely for this particle to be created.

However, if the attention is not only centred on the cases of direct production with no other particles created, other processes can be found which are substantially more probable:

2. Vector boson fusion: In this type of process [11], one of the quarks of one proton

would interact via a W^+, whereas one of the quarks of the other one would just interact with a Z^0, as shown in Figure 5, annihilating between them to create the resultant H^+. However, for this process, other final quarks still exist, so it does not verify the premise of "no additional particles created".

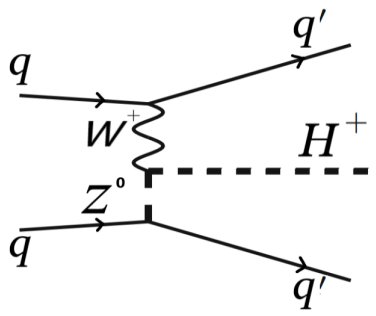

Figure 5: Feynman diagram of vector boson fusion to produce a charged Higgs H^+.

3. Furthermore, the H^+ boson could also be produced in pairs of charged $H^{\pm}$, with a 'Drell Yan like" process, in which one quark of each proton annihilate with each other, resulting in a photon γ or boson Z^0, which then decays into a pair of charged Higgs with opposite charge (Fig. 6).

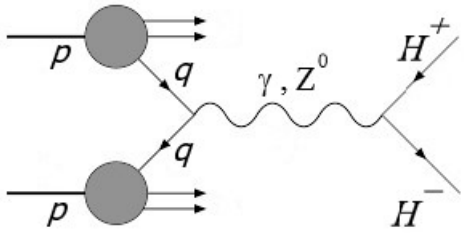

Figure 6: Feynman diagram of the production of pair of charged Higgs with opposite charges.

2.3 Decay processes

After being produced, this charged Higgs boson H^+can later spontaneously decay (this happens very fast, due to the mean life of the charged Higgs being extremely small) via different channels [7], but, as stated in the beginning, the only decay process that will be considered is:

$$H^+ \rightarrow \tau^+ + \nu_\tau \tag{9}$$

with the following Feynman diagram of Figure 7.

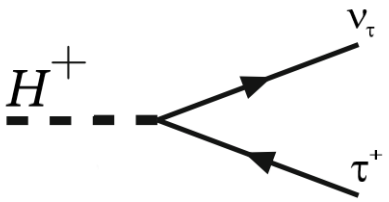

Figure 7: Charged Higgs boson decay to a tau τ^+ and neutrino ν_τ.

It could also be possible that the charged Higgs decayed to a pair of quarks:

$$\begin{aligned} H^+ &\rightarrow c\bar{s} \\ H^+ &\rightarrow c\bar{b} \\ H^+ &\rightarrow t\bar{b} \end{aligned} \tag{10}$$

or decays involving other bosons like:

$$\begin{aligned} H^+ &\rightarrow W^+\gamma \\ H^+ &\rightarrow W^+Z \end{aligned} \tag{11}$$

Notwithstanding the assumption of the decay to an antitau and tau neutrino, it is worth noting that this process is not the most favourable in most of the cases, because attending to the branching ratios of the different processes, a graphical representation like the one of Figure 8 can be found:

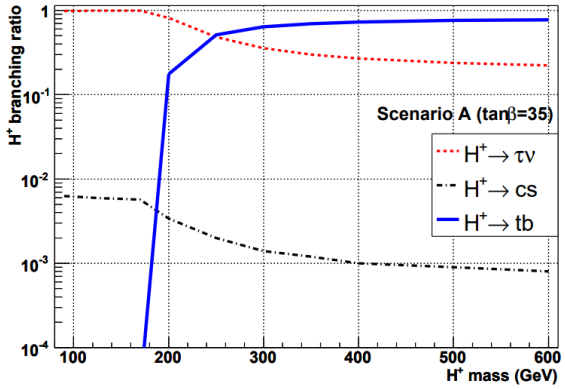

Figure 8: Branching ratios of H^+, for a $\tan\beta = 35$ in Type II 2HDM (taken from Ref.[12]).

where it can be observed that, for a mass of the charged Higgs m_{H^+} lower than the mass of the top quark t, the most favourable decay to occur is $H^+ \to \tau^+ + \nu_\tau$, whereas for a mass higher than the top quark, the decay $H^+ \to t\bar{b}$ becomes increasingly more dominant. Parallelly, the decay $H^+ \to c\bar{s}$ is more suppressed when the mass of the charged Higgs is higher than the top mass. This behaviour is due to the Yukawa coupling (see eq. (7)) between the different fermions and the Higgs field [13], which verifies that:

$$g_f \propto \frac{m_f}{v} \tag{12}$$

with m_f corresponding to the mass of a fermion f and $v = \sqrt{\frac{1}{\sqrt{2}G_F}} \approx 246$ GeV [14] is the vacuum expectation value for the Higgs field .

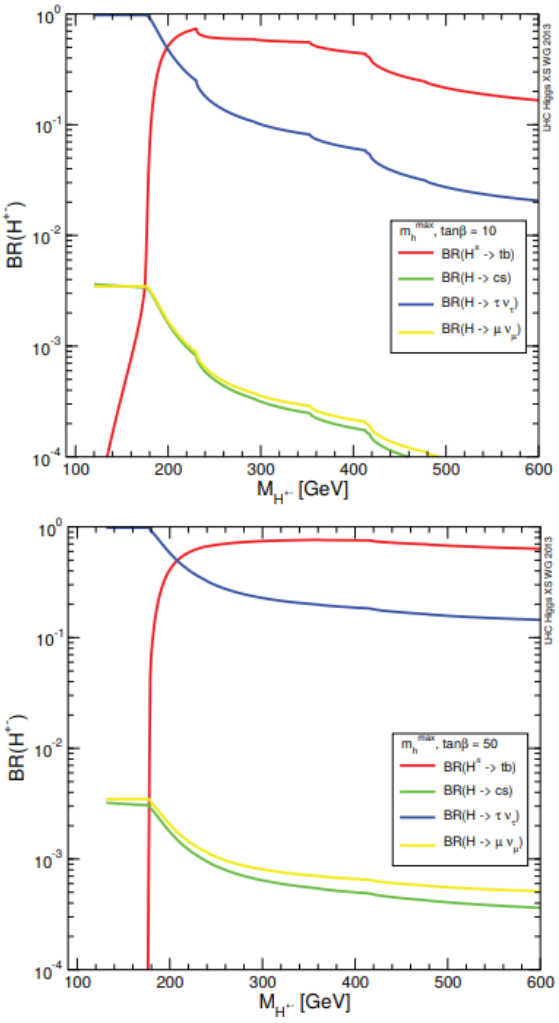

Figure 9: Branching ratios for different values of $\tan\beta$, in Type II 2HDM (taken from Ref.[15]).

This implies that, since the mass of the top quark is the biggest of all fermions, its coupling with the Higgs field is the strongest, and therefore its decay should be dominant. However, since the mass of the charged Higgs for this article is slightly bigger than the top mass m_t, attending to the graph of Figure 8, the process $H^+ \to \tau^+ + \nu_\tau$ should still remain dominant.

It can also be identified that the branching ratio for the $t\bar{b}$ channel does not increase abruptly after reaching $m_{H^+} = m_t + m_b$ (see Figure 9), but in reality it has to get to approximately $M = 200$ GeV/c^2 before becoming the main channel. This is mainly due to the kinematics of the processes, namely that, when sitting exactly on the threshold ($m_{H^+} = m_t + m_b$), there is zero phase space (which is a mathematical space of all the possible configurations of momenta of all the outgoing particles for the final states), and so this process is suppressed. However, for the leptons, the phase space is bigger, as there is more free energy for the final state (due too the sizeable mass difference between initial and final states), making the decays to this particles more favourable in certain occasions, as it has been visualised.

On the other hand, it must also be clarified that, attending to Figure 8, this interpretation has been made assuming a $\tan\beta = 35$. The Yukawa couplings are dependent on this parameter (see Table 1), and therefore, varying this magnitude produces significant changes to the previous graph of Figure 8, as it can also be appreciated in Figure 9, where changing the $\tan\beta$ from a value of 10 to a value of 50 has made the branching ratio for the decay to the tau and the neutrino clearly more sizable for masses of the charged Higgs bigger than the top quark mass m_t. This increase in the parameter $\tan\beta$ has also made the rise of the branching ratio for the $t\bar{b}$ channel become more abrupt than before.

The increase in $\tan\beta$ also makes the contribution of the other channels relevant for high masses of the charged Higgs, whereas for a small value of the parameter $\tan\beta = 10$, these channels became suppressed for masses $m_{H^+} > 500$ GeV/c^2,

And more in detail, for the decay of the charged Higgs to a tau τ^+ and neutrino ν_τ, setting a

mass of $M_{H^+} = 200$ GeV/c^2, the branching ratio changes as showed in Figure 10.

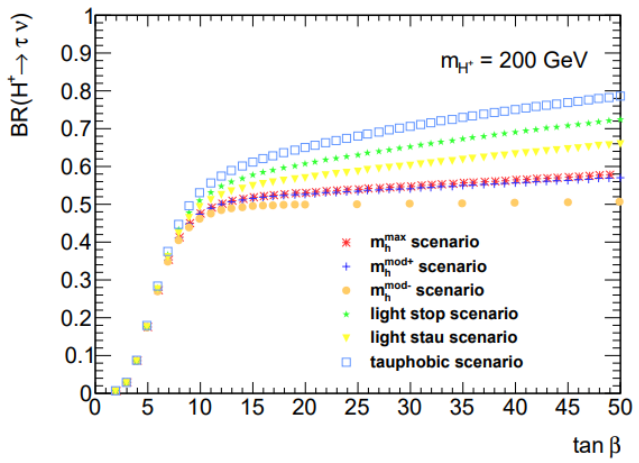

Figure 10: Branching ratio of the tau and netrino channels as a function of $\tan\beta$, at a $M_{H^+} = 200$ GeV/c^2 in Type II 2HDM (taken from Ref.[16]).

It can be discerned that, as the $\tan\beta$ grows, the branching ratio of the Higgs decaying to a tau and tau neutrino increases in consonance (it has an enhanced coupling to the tau at high $\tan\beta$ [7]). Notwithstanding that, it is also worth noting that for very low $\tan\beta$, the contribution of this channel to the total decay width Γ_{H^+} is minimal, not event accounting for 10% for $\tan\beta < 5$ at most.

3 Experimental procedure

3.1 Conservation laws

First of all, as it was mentioned in the beginning, a head-on collision of two protons going in opposite directions is considered in this experiment, and therefore, it is assumed that the transverse momentum of both quarks taking part in the annihilation is null ($\vec{p_T} = 0$). However, in reality, a lot of quark-antiquark pairs are constantly formed in the quark sea of the protons, which can have a considerable transversal momentum, and after colliding with a valence quark of the other proton, could in theory produce a charged Higgs with noticeable transverse momentum. Nevertheless, this phenomenon is tremendously improbable, so it will be assumed that both quarks collide travelling on the beam axis, resulting in a charged Higgs which will move on this same axis to conserve linear momentum. As for its direction of motion, the u quark will presumably carry a bigger momentum than the d quark attending to its PDF (see that the distribution function for the u quark is always higher than the one of the d, so it is more probable that the resultant Higgs moves pointing to the direction that followed the incident u quark). It should additionally be noted that the protons cannot perfectly collide with each other at a zero angle, but this asymmetry has been reduced considerably (to approximately 150 mrad[17])

As for the momenta of the leptons τ and ν_τ produced in the decay of the Higgs, if the Higgs rest frame is considered (i.e. $\vec{p}_{H^+} = 0$), then they both will have the same modulus for their momenta but pointing in opposite directions, i.e. $\vec{p}_\tau = -\vec{p}_{\nu_\tau}$ to verify the conservation of linear momentum.
Now, considering that the Higgs is a scalar with spin $S = 0$ [18], having a look at the conservation of total angular momentum:

$$\vec{J} = \vec{L} + \vec{S} \tag{13}$$

If the Higgs is studied from its rest frame ($\vec{p}_H$=0), with a consequent angular momentum of 0, then the conservation of total angular momentum follows as:

$$\vec{J}_H = \vec{J}_{\tau+\nu_\tau}$$

For the Higgs boson, a total angular momentum is obtained, attending to eq. (13), of:

$$\vec{J}_H = \vec{L}_H + \vec{S}_H = 0 + 0 = 0$$

On the other hand, for the leptons (with $s = 1/2$):

$$\vec{J}_{\tau+\nu_\tau} = \vec{L} + \vec{S_\tau} + \vec{S_{\nu_\tau}}$$

As a result, if the conservation of $\vec{J}$ is evaluated, we get that the quantum number ℓ must be:

$$\ell = 0, 1$$

From the two possible ℓ values, the configuration of $\ell = 0$ is correct, which corresponds to a state s, involving that there is no dependence on the angles, and therefore there is a radial symmetry. This also implies that the angular distribution of the leptons produced from the decay of the H^+

should be uniform and constant for all the angles, and therefore there should not be a preferred direction for the decay to happen.

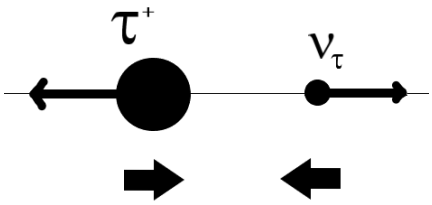

Figure 11: Scheme of the decay, indicating the direction of the momentum and spin of the particles.

Also, taking into account the distribution of the leptons in the decay pointing in opposite directions, and considering that neutrinos ν (and in general fermions) must have a left-handed chirality [19], as these are the ones observed in nature, the tau τ must have a left-handed helicity to verify the conservation of total angular momentum.

3.2 Energy and momentum relations

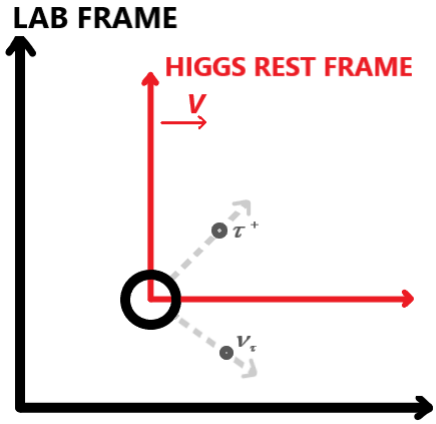

Figure 12: Graphical representation of both the laboratory and the Higgs rest frame.

Now, being in the Higgs rest frame, the energy of the tau τ^+ could be calculated in that frame, with the use of 4-momenta:

$$\begin{aligned}
&(P_H^\mu - P_\tau^\mu)^2 = P_{\nu_\tau}^\mu P_{\nu_\tau}^\mu = M_{\nu_\tau}^2 = 0 \\
&P_H^\mu P_H^\mu + P_\tau^\mu P_\tau^\mu - 2P_H^\mu P_\tau^\mu = 0 \\
&M_H^2 + M_\tau^2 - 2(E_H^* E_\tau^* - \vec{p_H}\vec{p_\tau}) = 0 \\
&M_H^2 + M_\tau^2 - 2(M_H E_\tau^*) = 0
\end{aligned}$$

$$\implies E_\tau^* = \frac{M_H^2 + M_\tau^2}{2M_H} \tag{14}$$

Knowing the expression for the energy in the Higgs rest frame given by eq. (14), it can be estimated for the mass of the charged Higgs initially considered of $M_{H^+} = 200$ GeV/c^2, obtaining:

$$E_\tau^* = 100.1 \text{ GeV}$$

On the other hand, if it was required to calculate the velocity coefficient $\beta = v/c$ of the Higgs in the laboratory frame, as a function of E_τ^*, i.e. the energy in the rest frame, with the Higgs moving on the z-axis at a velocity $\vec{v} = (0, 0, v)$, a Lorentz transformation should be applied, which follows the equation [20]:

$$E_\tau^* = \frac{E_\tau - v p_{\tau,z}}{\sqrt{1 - v^2/c^2}} = \frac{E_\tau - \beta c p_{\tau,z}}{\sqrt{1 - \beta^2}} \tag{15}$$

getting from eq. (15) that:

$$E_\tau^{*2} = \frac{E_\tau^2 - 2E_\tau \beta c p_{\tau,z} + \beta^2 c^2 p_{\tau,z}^2}{1 - \beta^2}$$

$$E_\tau^{*2} - \beta^2 E_\tau^* = E_\tau^2 - 2E_\tau \beta c p_{\tau,z} + \beta^2 c^2 p_{\tau,z}^2 = 0$$

$$\beta^2(c^2 p_{\tau,z}^2 + E\tau^{*2}) + \beta(-2E_\tau c p_{\tau,z}) + (E_\tau^2 - E_\tau^{*2}) = 0$$

$$\beta = \frac{E_\tau c p_{\tau,z} \pm \sqrt{c^2 p_{\tau,z}^2 E_\tau^{*2} - E_\tau^{*2} E_\tau^2 + E_\tau^{*4}}}{(c^2 p_{\tau,z}^2 - E_\tau^{*2})} \tag{16}$$

and, so, a relation is obtained between the velocity coefficient β, the energies of the tau τ in both frames and its momentum p_τ (the subindex z indicates that only the z-component has to be considered).

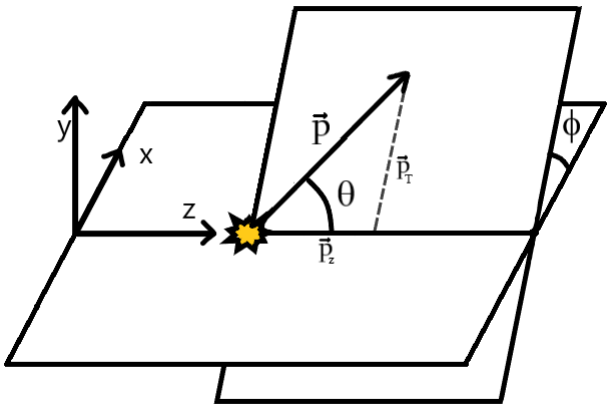

Figure 13: Scheme showing the θ and ϕ angles.

One could also wonder what would happen to the polar angle θ, i.e., the angle between beam axis and tau momentum, being measured from both the laboratory to the Higgs rest frame.
To find the value for this angle in the Higgs rest frame, which will be denoted as θ^*, it is known that [20]:

$$\tan(\theta^*) = \frac{p^*_\perp}{p^*_\parallel} \quad \begin{cases} p^*_\perp = p_\perp \\ p^*_\parallel = \gamma(p_\parallel - vE_\tau/c) \end{cases}$$

where $p_\perp$ and $p_\parallel$ correspond to the perpendicular and parallel momentum component, respectively, of the tau in the laboratory frame, γ the Lorentz factor of the Higgs and v its velocity.
Substituting both components:

$$\tan(\theta^*) = \frac{p^*_\perp}{p^*_\parallel} = \frac{p_\tau \sin\theta}{\gamma(p_\tau \cos\theta - \beta E_\tau/c)} \tag{17}$$

Other relevant magnitudes for the particle decay, which will help with the posterior analysis, are the azimuthal angle ϕ , defined as the angle around the beam axis, and the pseudorapidity, which describes the angle between the momentum of a particle and the beam axis:

$$\eta = -\ln\left[\tan\left(\frac{\theta}{2}\right)\right] \tag{18}$$

Consequently, particles with high values of η, or similarly with small angles, are close to the beam axis (as seen in Figure 14), and, hence, will have trouble being recorded, as it will be explained later.

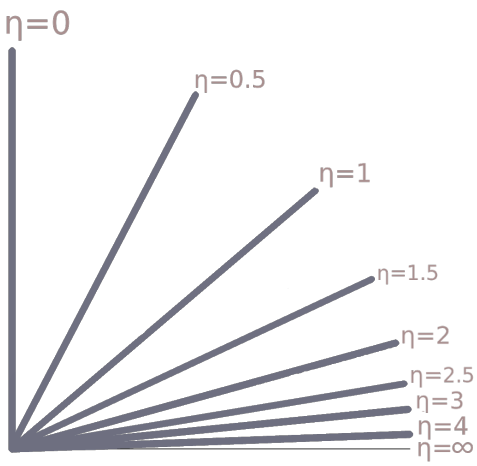

Figure 14: Pseudorapidity values shown on a polar plot.

As mentioned before, the Higgs is a very unstable particle, which tends to decay very quickly (this being the reason why it is more convenient to study its decays), with a decay width of $\Gamma_H \sim 1$ GeV, which is the probability per unit of time of the particle decaying. This width is, in reality, the sum of numerous partial decay widths which can be added up linearly, as seen in eq. (19)

$$\begin{aligned}\Gamma_{H^+} = \Gamma_{H^+\to\tau^+\nu_\tau} + \Gamma_{H^+\to\mu^+\nu_m u} + \Gamma_{H^+\to t\bar{b}} \\ +\Gamma_{H^+\to t\bar{s}} + \Gamma_{H^+\to t\bar{d}} + \Gamma_{H^+\to c\bar{b}} + ...\end{aligned} \tag{19}$$

which in the end contribute to widen the natural decay width. As seen in Figure 15, this magnitude corresponds to a parameter of a relativistic Breit–Wigner distribution (this curve describes the distribution of masses that a particle at the LHC takes when it is created), in which M is the mass of the initial state, E the energy of the decay products and σ the cross section for each energy E. Analytically, the decay width of the particle is correlated to the Heisenberg's uncertainty principle as follows:

$$\Gamma = 2\Delta E = \frac{\hbar}{\tau} \tag{20}$$

as a consequence of the uncertainty principle $\Delta E \Delta t \geq \frac{\hbar}{2}$.

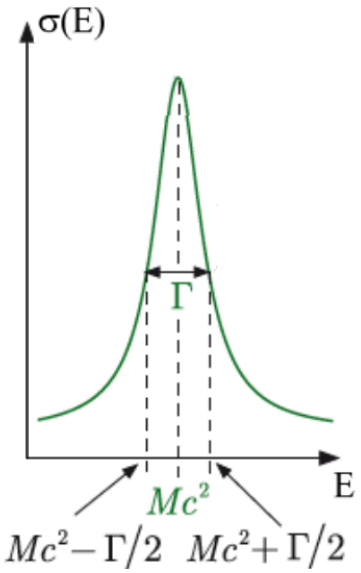

Figure 15: Graphical representation of the natural decay width.

For that reason, using eq. (20) , a resultant lifetime of the charged Higgs is obtained of:

$$\tau_{H^+} = \frac{\hbar}{\Gamma_{H^+}} = 6.59 \cdot 10^{-25} \text{ s}$$

which is even shorter than the lifetime associated to the Higgs, measured at $\tau_{H^0} = 2.1^{+2.3}_{-0.9} \cdot 10^{22}$ s [21]. Therefore, as a result of the interpretation of Figure 15, this width corresponds to an uncertainty in M of:

$$\sigma_{M_H} \sim \frac{\Gamma}{2} = 0.5 \text{ GeV}$$

Knowing the uncertainty associated to the mass M_H, it is possible to determine the derived uncertainty for other magnitudes[1]. For instance, the error for the angle θ^* can be computed, as shown with eq. (22) in Appendix B.

3.3 Reading LHE file

With these calculations in mind, the previous results can be applied to the analysis of a sample of LHC events, given as a Les Houches Events File (LHE), a standard format used to organise all the information necessary to characterise a particle interaction. In this type of files, one can access information about the masses, energies, momenta, and other magnitudes that help simulate the process to analyse, which in the case that concerns this project corresponds to the decay of the charged Higgs after the proton-proton collision.

To analyse the data gathered in the LHE file, the Python module *lhereader.py* [22] can be employed, that reads the information of each event in the Les Houches Events format (see Figure A.1 in Appendix), and converts it to a more understandable format (see Figure A.2 in Appendix), where the following information can be found:

1. *pdgid*: Particle Data Group ID, which follows the Monte Carlo particle numbering scheme [23], assigning a number to each particle so that it facilitates the particle identification in particle event generators, detector simulators or other simulators of the same nature. The numbers for the different particles in the events analysed for the charged Higgs decay are: $\bar{s} \to -3$, $c \to 4$, $H^+ \to 37$, $\tau^+ \to -15$ and $\nu_\tau \to 16$.

2. p_x, p_y and p_z: momentum components of each of the particles.

3. Other information about the *spin*, *mass* and *energy* of each of the particles.

After processing all the information with the Python module *lhereader.py* , the polar angle θ and azimuthal angle ϕ can be computed, and other magnitudes like the velocity coefficient β, among others.
Moreover, having access to all the information about each of the particles, cuts can be applied to the different magnitudes, which will be useful in the future to select the events that are convenient for the data analysis, making restrictions mainly

[1]For this calculation, it is assumed that everything measured is known with perfect precision, and that the only source of uncertainty is the Higgs mass.

on the transverse momentum p_T and the pseudo-rapidity η, to maximize the efficiency of the event detection.

3.4 Events generation

After having processed the events of the provided LHE file, the next step would be to generate a process on our own by means of the particle collision simulator *MadGraph5* [24, 25, 26], that allows the computation of the cross section (and branching ratios) and generation of events for any process. The procedure to follow to generate the events would be as follows:

1. First, download and install all the *MadGraph* software, with the programs *Pythia8* (which helps with the hadronization of the events), *MadAnalysis* (for the posterior analysis of the data), *MadSpin* (for the later computation of cross sections and branching ratios), etc.

2. Then, go to the terminal and type "./bin/mg5_aMC", which should make the program run.

3. Since the Standard model is not being used, the correct model should be imported as: "import model 2HDM". This will add the charged Higgs boson to the zoo of particles in the database.

4. Finally, the particle decay to examine is introduced, specifying the particles in the process: "generate $pp > h+ >$ ta+ vt ". It must be clarified that, although it was mentioned in the beginning of the project that the $t\bar{b}$ annihilation can create a charged Higgs, this process will not be considered, as these quarks do not exist inside the proton.

5. After that, the events are generated using: "output ChargedHiggs", which created a directory called *ChargedHiggs* with all the information necessary to create the events, and later, "launch ChargedHiggs", which proceeds to generate a run of events.

6. Eventually, the program will require the user to specify if he wants to make any changes to the parameters *param_card.dat* or the run card *run_card.dat*, creating the process in the end.

On the other hand, the Feynman diagrams for the different allowed processes can also be accessed, and the LHE file can be extracted in the end.

4 Results and analysis

4.1 Angular distributions in the laboratory frame

Using the data extracted from the LHE file [27], the angular distribution of the polar angle can be computed and, later on, plotted as the number of events N versus the polar angle θ, obtaining the graphical representation of Figure 16.

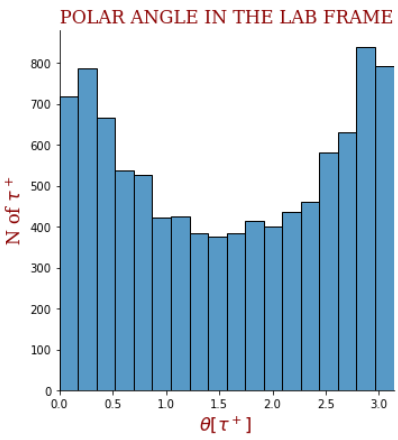

Figure 16: Polar angle distribution of the tau in the lab frame.

where it can observed that this angular distribution is not uniform, with a higher number of events concentrated for small angles were $\theta \to 0$ and for big angles where $\theta \to \pi$, with both angles meaning that there is a preferred direction for the tau τ^+ to decay oriented on the beam axis. A similar representation can be plotted for the azimuthal angle ϕ, which results in the graph of Figure 17.

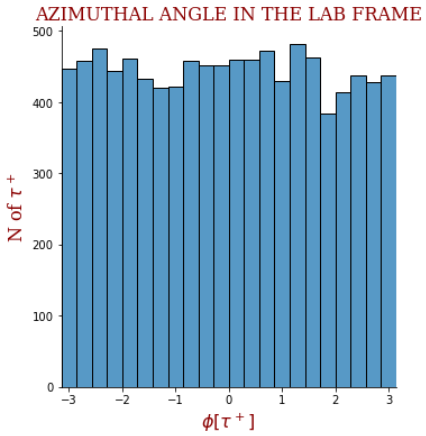

Figure 17: Azimuthal angle distribution of the tau in the lab frame.

Differently to what happens for the polar angle, looking at the azimuthal angle plot in the laboratory frame, it can be stated that the angular distribution is uniform for all angles (there is little fluctuations due to the probabilistic nature of the decay, but they can be considered negligible). Alternatively, the pseudorapidity, obtained by means of eq. (18), is plotted in Figure 18:

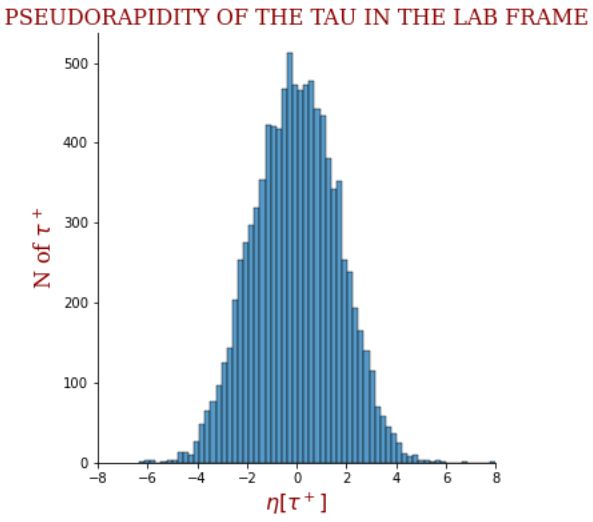

Figure 18: Pseudorapidity of the tau in the lab frame.

One more time, it can be appreciated that the curve for the pseudorapidity is very wide, with many events with an η over 1.5, so there is a preferred orientation to decay very close to the beam axis, corresponding to a polar angle of $\theta < 25$.

4.2 Angular distributions in the Higgs rest frame

Similarly for the Higgs rest frame, the following plots can be obtained for the polar angle θ^*, azimuthal angle ϕ^* and pseudorapidity η^*, represented in Figures 19, 20 and 21, respectively:

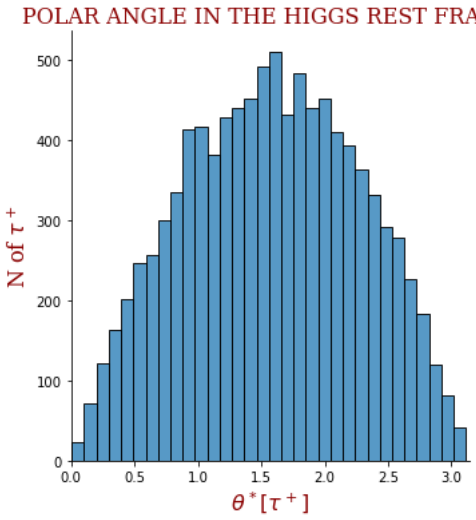

Figure 19: Polar angle distribution of the tau in the HIggs rest frame.

where it can be observed that, after applying the Lorentz transformation to the polar angle, the graphical distribution has changed completely, with angles close to the beam axis becoming extremely unlikely to occur.

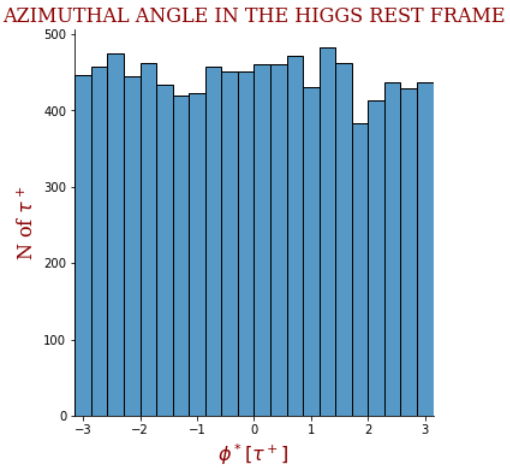

Figure 20: Azimuthal angle distribution of the tau in the Higgs rest frame.

However, there is no change in the azimuthal angle distribution from one frame to the other, remaining uniform over all angles.

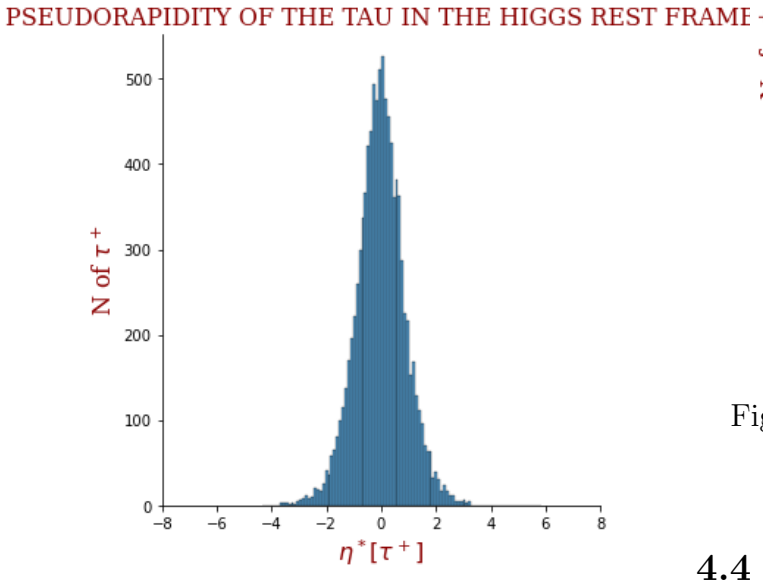

Figure 21: Pseudorapidity of the tau in the Higgs rest frame.

For the pseudorapidity, it can be identified, while comparing with the pseudorapidity in the lab frame, that the angular distribution of the τ^+ is now more likely to be oriented perpendicularly to the beam axis, given that the function of η has become dramatically narrower.
These observations can later be observed graphically in Figures 24 and 25, where the direction of the momentum of the tau with respect to the beam axis is clearly visible.

4.3 Velocity coefficient

And finally, the velocity coefficient can also be computed to obtain the velocity distribution of the tau, which results in the Figure 22, with a large number of τ^+ moving close to the speed of light c.

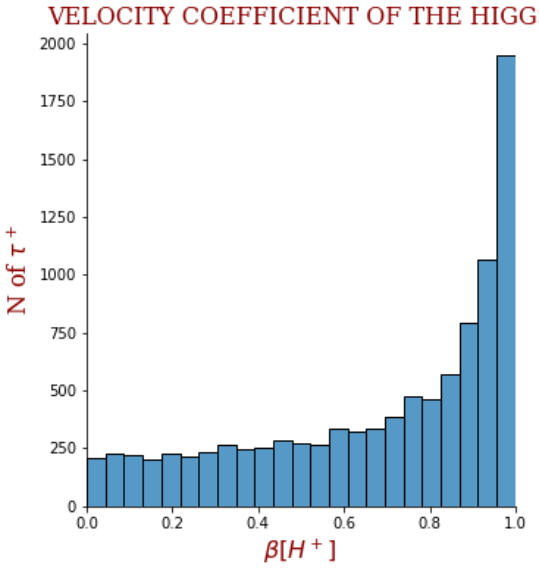

Figure 22: Velocity coefficient of the Higgs.

4.4 Generation of events

After having generated the events for the pertinent process ($pp \to H^+ \to \tau^+\nu_\tau$), the analysis of the obtained results and the comparison with the LHE file provided [27] can be carried out. After doing that, it is found that, probably because of a misseting of the cuts or the different parameters, all the events in the provided LHE file corresponded to a $c\bar{s}$ annihilation, with no pairs of $u\bar{d}$ appearing in any of the events. Consequently, no information about the probabilities of each of the processes taking place could be extracted.

However, for the new generated LHE file, both the $u\bar{d}$ and the $c\bar{s}$ annihilations were considered (since this is what actually happens for a proton-proton collision), for a $\tan\beta = 50$ in the framework of the Type II model, measuring in each case the number of events displayed in Table 2 from a total of $N = 10000$ events.

Quark pair	Number of events
$c\bar{s}$	1157
$u\bar{d}$	8843

Table 2: Number of events for each quark pair, for a run of $N = 10000$ events.

For this first run of events, simulating the production of the charged Higgs after collision, a cross section was estimated, using the *Madgraph* program, of:

$$\sigma_{N=10000}(pp \to H^+) = (2.571 \pm 0.003) \cdot 10^4 \text{ pb}$$

For comparison, the same process was generated for a larger number of events, of $N = 500000$, obtaining the results displayed in Table 3.

Quark pair	Number of events
$c\bar{s}$	56936
$u\bar{d}$	443064

Table 3: Number of events for each quark pair, for a run of $N = 500000$ events.

Again, the cross section was estimated, which resulted in a value of:

$$\sigma_{N=500000}(pp \to H^+) = (2.57087 \pm 0.00012) \cdot 10^4 \text{ pb}$$

Parallelly, the individual cross sections for both quark annihilations were computed, obtaining the results organised in Table 4.

Quark pair	σ [pb]
$c\bar{s}$	1476.0±1.1
$u\bar{d}$	11112±12

Table 4: Cross sections for both quark annihilations, for the run of $N = 500000$ events.

Since the representation of the angular distributions should lead to the same results, as it was later verified (see [28]), the analysis of the generated events mainly focused on the calculation of the decay width, cross sections and branching ratios of the different decay processes. After computing these magnitudes with the program *MadSpin*, for the run of $N = 500000$ events (which should give more precise estimations), the values organised in Table 5 are obtained:

Particles	BR
$\tau^+ \nu_\tau$	0.468
$t\bar{b}$	0.325
$\mu^+ \nu_\mu$	0.068
$c\bar{s}$	0.065
$u\bar{d}$	0.049
$e^+\nu_e$	0.025
Particles	$BR \cdot 10^4$
$u\bar{s}$	0.72
$c\bar{d}$	0.68
$u\bar{d}$	0.50
$c\bar{b}$	0.03
$e^+\nu_\tau$	0.06
$\mu^+\nu_\tau$	0.06
$e^+\nu_\mu$	0.06
$\tau^+\nu_\mu$	0.06
$\mu^+\nu_e$	0.06
$\tau^+\nu_e$	0.06
$t\bar{s}$	0.03
$t\bar{d}$	0.02

Table 5: Branching ratio BR for each possibility of final particles.

Besides that, the program also provides a decay width for the process of:

$$\Gamma_{H^+} = 61.5 \text{ GeV}$$

And for each of the decays, the partial decay widths of Table 6 can be computed individually employing the *Madgraph* program.

Particles	Γ_i [GeV]
$\tau^+\nu_\tau$	28.78
$t\bar{b}$	19.99
$\mu^+ \nu_\mu$	4.18
$c\bar{s}$	4.00
$u\bar{d}$	3.01
$e^+\nu_e$	1.54

Table 6: Partial decay width Γ_i for each possibility of final particles (only de main decay channels are considered).

5 Discussion

5.1 Angular distributions

Looking at the plots of the angular distributions in the Higgs rest frame (Figures 19 and 20), it is found that the decay angle is actually uniform in this frame, as the graphical representation follows a cosine function. This happens because, as the decay direction is isotropic, each element of solid angle must have the same probability of containing the direction of the τ^+, and, therefore, this isotropic distribution must be regularly distributed over the cosine of the polar angle θ.

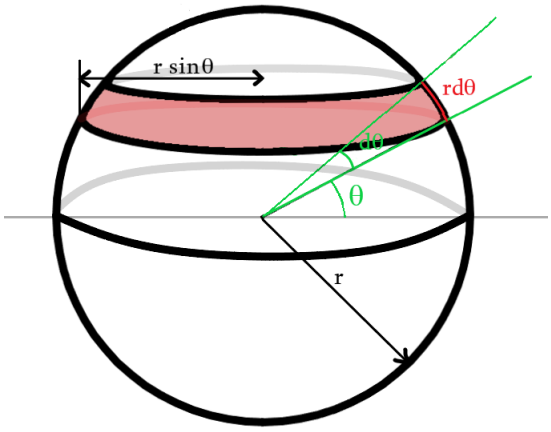

Figure 23: Reference image to explain the isotropic angular distribution of the decay.

To understand this analytically, it is assumed that an sphere of radius r (with center on the point where the Higgs decays) surrounds the point of collision (see Figure 23. Now, it is found that the area that solid angle that subtends a ring from θ to $\theta + d\theta$ is:

$$d\Omega = \frac{A_{ring}}{r^2} = \frac{2\pi(r\sin\theta)(rd\theta)}{r^2} =$$

$$= 2\pi\sin\theta d\theta = -2\pi d(\cos\theta) \qquad (21)$$

As a result, the angular distribution in the Higgs rest frame must have the form of a cosine, as it can be seen in Figure 19. In order to comprehend this easily, one can have a look at the angular distributions in polar coordinates for both frames:

- **Laboratory frame:**

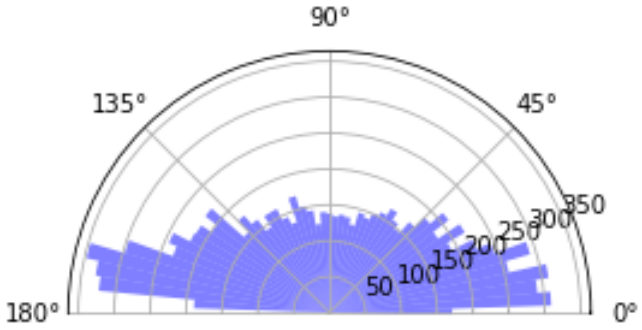

Figure 24: Angular distribution in the laboratory frame with polar coordinates.

For this frame, the distribution has a higher number of events concentrated, as explained before, along the beam axis (preferred direction), with fewer events at more perpendicular angles.

- **Higgs rest frame:**

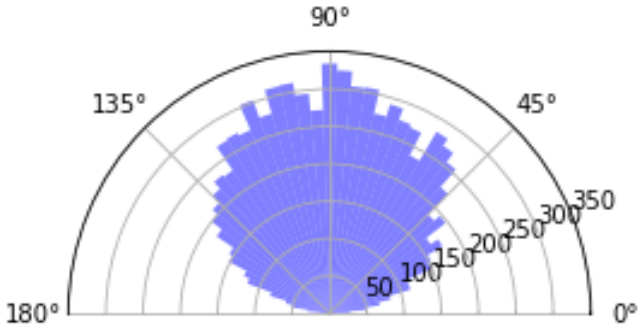

Figure 25: Angular distribution in the Higgs rest frame with polar coordinates.

The graph follows a Lambertian distribution, as it would be called in optics, so that there is no preferred direction of motion for the τ^+, since for this distribution the "radiance" is uniform measured from every orientation. The decay of the charged Higgs is, as a result, could be seen as a perfect Lambertian emitter [29].

Alternatively, it can be chosen to plot the cosine of the angle $\cos\theta^*$ instead of the angle θ^*, as the isotropic angular distribution of the tau τ^+ should be flat for this magnitude, as it can be recognised in Figure 26.

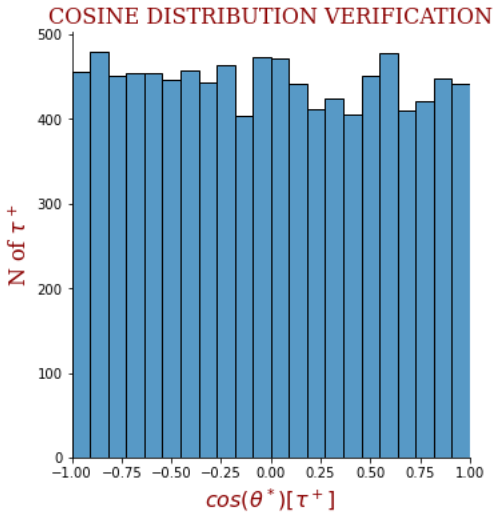

Figure 26: Verification of the uniformity of the angular distribution in the particle decay.

5.2 Geometry of the detector

On the other hand, it can be easily seen in Figure 16 that, after the collision, most of the particles come up at small angles of θ approaching zero, i.e., really close to the beam axis. However, the fact that the resultant particles are pointed in these directions is not convenient, attending to the geometry of the detector the LHC works with, schematically shown in Figure 27.

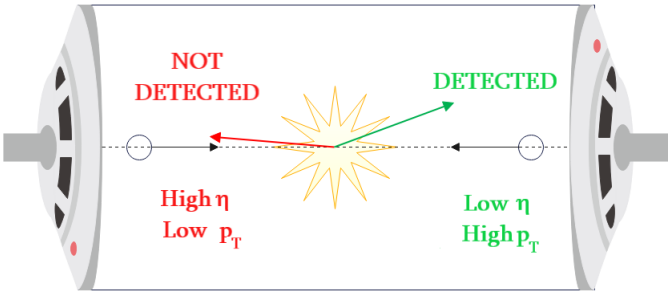

Figure 27: Scheme of the detector.

In the LHC, both particle beams travel in the interior of beam pipes – two tubes kept at ultra-high vacuum, until they reach the detector where they collide. As a result, if after the collision the particles have small transverse momentum (or, alternatively, big pseudorapidity) it might be possible that the particles travel back through the same beam, not being detected by the silicon strip tracker of the CMS or leading to wrong detections [30]. To prevent this from happening, it is convenient to apply some cuts to the gathered data: for the transverse momentum $p_T > 10$ GeV/c and for the pseudorapidity $|\eta| < 2.5$, as these are approximately the limitations that the CMS detector has [31, 32], obtaining this time the following plots for the angular distributions:

- **Laboratory frame.** Looking first at the angular distributions for the laboratory frame, the plots of Figures 28 and 29 are extracted.

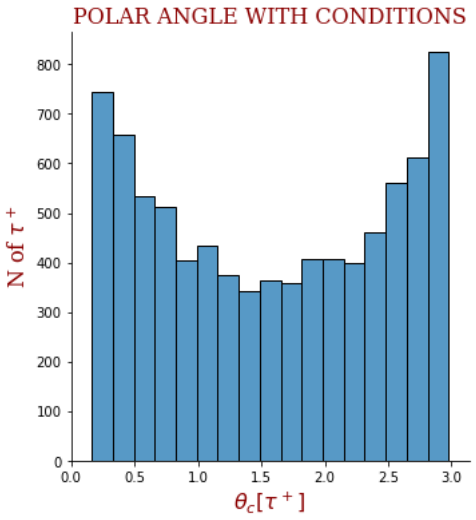

Figure 28: Polar angle in the lab frame applying the conditions mentioned.

As it can be appreciated in the plot of the polar angle of Figure 28, the angular distributions has been suppressed for small angles, so, in theory, all these processes shown should be detected without any problems, as the momentum of the tau cannot point to the beam pipe.

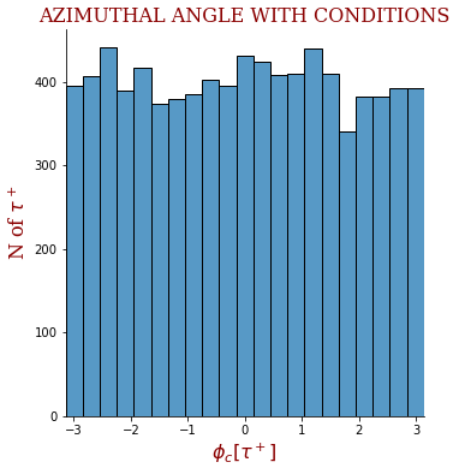

Figure 29: Azimuthal angle in the lab frame applying the conditions mentioned.

The angular distributions of the azimuthal angles, nonetheless, remain invariant after applying these cuts, as this angle is contained in the x-z plane

- **Higgs rest frame.** Considering the Higgs rest frame, and applying the same conditions, the graphs of Figures 30 and 31 can be plotted.

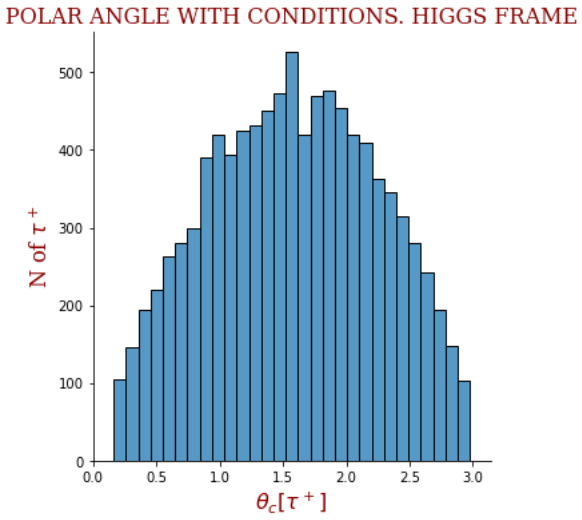

Figure 30: Polar angle in the Higgs rest frame applying the conditions mentioned.

Similarly for the Higgs rest frame, the events at small angles have been discarded, not fulfilling the conditions imposed, again making sure that the remaining events can be measured by the detector.

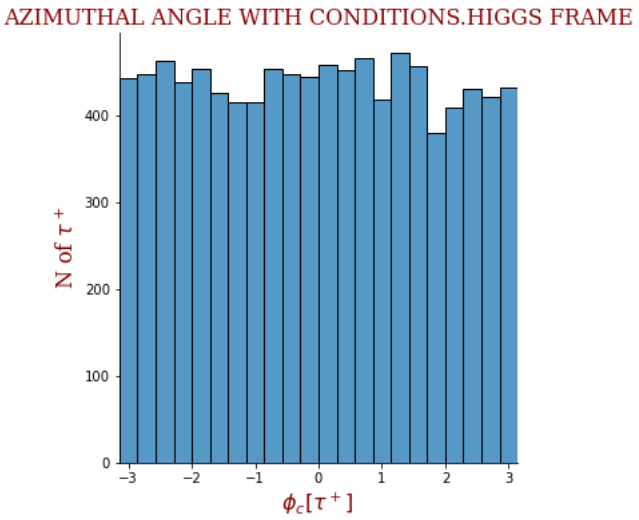

Figure 31: Azimuthal angle in the Higgs rest frame applying the conditions mentioned.

Analogously to the laboratory frame case, the angular distribution of the azimuthal angle applying the conditions does not change for the same reason as it was explained before.

5.3 Generation of events

After having obtained the statistical results for the events generated about the production and decay of the charged Higgs, these results allow to confirm the validity of the initial suppositions extracted from the examination of the PDF of the proton, that is to say, that the $u\bar{d}$ annihilation is considerably more probable, with a ratio between the number of events for both cases of:

$$R_1 = \frac{\sigma(c\bar{s} \to H^+)}{\sigma(u\bar{d} \to H^+)} \approx 0.1308 \text{ for N=10000 events}$$

which, as explained before, is due to a higher probability density for both the u and d valence quarks, and a higher probability of $u\bar{u}$ and $d\bar{d}$ virtual pairs inside the proton being created, as the parton distribution functions of these quarks are certainly higher than those of the heavier quarks (see, for instance, that the heaviest possible quarks inside the proton, the bottom quark, has the lowest PDF). For comparison, and to get a more precise value

for this ratio, the same process was generated for a number of $N = 500000$ events (see [28]), obtaining:

$$R_2 = \frac{\sigma(c\bar{s} \to H^+)}{\sigma(u\bar{d} \to H^+)} \approx 0.1285 \text{ for N=500000 events}$$

These ratios are in good agreement with the one which would be extracted by merely dividing the cross sections provided by the *Madgraph* software, which would give a result of $R_3 = 0.1328$, with small discrepancies between all values, that in any case account for more than 3.35 %, and with the cross sections having minimum relative errors close to 0.1 % The results also show the importance of considering the sea quarks, instead of just the valence quarks of the protons, as the annihilations of this nature account for more than 10% of all the production processes generated, and therefore cannot be neglected.

As for the estimated cross section for both runs of 10000 and 500000 events, of $\sigma(pp \to H^+) = (2.571 \pm 0.003) \cdot 10^4$ pb and $\sigma(pp \to H^+) = (2.57087 \pm 0.00012) \cdot 10^4$ pb, respectively, they are both certainly close, with discrepancies between them of just 0.005 % that point out that these values are relatively accurate. One can also notice, attending to these cross sections, that the quark annihilation is not, as enumerated in the beginning, the only production channel for the charged Higgs:

$$\frac{\sigma(c\bar{s} \to H^+) + \sigma(u\bar{d} \to H^+)}{\sigma(pp \to H^+)} = 0.4896$$

proving the existence of other production channels like the vector boson fusion and Drell-Yang processes, among others, which would correspond to more than 50% of the events.

Now looking at the decay processes, as it was expected for a mass of $M_{H^+} = 200$ GeV/c^2, the three main decay channels are $\tau^+\nu_\tau$, $t\bar{b}$ and $\mu^+\nu_\mu$. The reason why other quark decays like $u\bar{s}$ or $c\bar{d}$, among others, are less probable is due to its differences in decay widths:

$$\frac{\Gamma(H^+ \to c\bar{d})}{\Gamma(H^+ \to c\bar{s})} \propto \frac{|V_{cd}|^2 m_d^2}{|V_{cs}|^2 m_s^2} = 3.35 \cdot 10^{-4}$$

so, this process is Cabibbo suppressed, having a much lower probability to happen than the ones involving the CKM matrix diagonal elements, i.e. the processes with $u\bar{d}$, $c\bar{s}$ and $t\bar{b}$ vertices, which are, on the contrary, enhanced (remember that the CKM matrix elements have values very close to one). The reason why the $t\bar{b}$ channel is not the main decay channel might be, as explained in the beginning, that this process is not kinematically favoured for the mass of the charged Higgs assumed in this project, although it is reasonably likely that this decay becomes dominant if the mass increases (as it was seen in Figure 8).
The estimated values for all the branching ratios of the charged Higgs are in good agreement with the theoretical predictions proposed in the Introduction, and therefore, the results can be considered satisfactory.

With respect to the decay width computed for the charged Higgs, of $\Gamma = 61.5$ GeV, it must be mentioned that this value is exceedingly high, so caution should be exercised when considering this as a reliable result, considering that other massive particles like the top quark t has a predicted decay width in the Standard Model of just $\Gamma_t = 1.32$ GeV [33].

6 Conclusions

The production and decay processes of the charged Higgs boson H^+ have been analysed, applying conservation of linear and total angular momentum to predict the angular distribution of its decays. These predictions have been verified via the processing of the events gathered in an LHE file, which have allowed to study the nature of particle decays. After that, the same process has been studied by means of the use of an event generator, which has eventually provided information about the cross sections and branching ratios of the different production and decay processes.

Appendices

A LHE files.

```
<event>
 5   0  0.1170000E-07  0.2007119E+03  0.7816531E-02  0.1149140E+00
       -3   -1    0    0    0  501  0.00000000000E+00  0.00000000000E+00  0.98858873129E+02  0.98858928890E+02  0.12500000000E+01 0.  1.
        4   -1    0    0  501    0  0.00000000000E+00  0.00000000000E+00 -0.10186786837E+03  0.10187553733E+03  0.10499999672E+00 0.  1.
       37    2    1    2    0    0  0.00000000000E+00  0.00000000000E+00 -0.30089952384E+01  0.20073446622E+03  0.20071191264E+03 0.  0.
      -15    1    3    3    0    0  0.20662917874E+02  0.83965590618E+02  0.49418318949E+02  0.99611769181E+02  0.17769999504E+01 0. -1.
       16    1    3    3    0    0 -0.20662917874E+02 -0.83965590618E+02 -0.52427314187E+02  0.10112269704E+03  0.00000000000E+00 0. -1.
</event>
```

Figure A.1: LHE original data format.

```
EVENT NUMBER 9780
Particle(pdgid=-3, px=0.0, py=0.0, pz=98.858873129, energy=98.85892889, mass=1.25, spin=1, status=-1, vtau=0.0, parent=-1)
Particle(pdgid=4, px=0.0, py=0.0, pz=-101.86786837, energy=101.87553733, mass=0.10499999672, spin=1, status=-1, vtau=0.0, parent=-1)
Particle(pdgid=37, px=0.0, py=0.0, pz=-3.0089952384, energy=200.73446622, mass=200.71191264, spin=0, status=2, vtau=0.0, parent=0)
Particle(pdgid=-15, px=20.662917874, py=83.965590618, pz=49.418318949, energy=99.611769181, mass=1.7769999504, spin=-1, status=1, vtau=0.0, parent=2)
Particle(pdgid=16, px=-20.662917874, py=-83.965590618, pz=-52.427314187, energy=101.12269704, mass=0.0, spin=-1, status=1, vtau=0.0, parent=2)
```

Figure A.2: LHE processed data format after using Python module.

B Uncertainty estimation.

$$\sigma_{\theta^*} = \sqrt{\left(\frac{\partial\theta^*}{\partial M_H}\right)^2 \sigma_M^2} = \sigma_M \sqrt{\left(\frac{\partial\theta^*}{\partial\beta}\right)^2 \left(\frac{\partial\beta}{\partial M_H}\right)^2 + \left(\frac{\partial\theta^*}{\partial\gamma}\right)^2 \left(\frac{\partial\gamma}{\partial\beta}\right)^2 \left(\frac{\partial\beta}{\partial M_H}\right)^2} \tag{22}$$

where it can be obtained that:

$$\left(\frac{\partial\theta^*}{\partial\gamma}\right) = -\frac{p_T c \left(p_\parallel c - E\right)}{p_T^2 c^2 + \gamma^2 \left(p_\parallel c - E\right)^2}$$

$$\left(\frac{\partial\theta^*}{\partial\beta}\right) = \frac{p_T \gamma E_\tau c}{p_T^2 c^2 + \gamma^2 \left(p_\parallel c - \beta E_\tau\right)^2}$$

and, in the same way:

$$\left(\frac{\partial\gamma}{\partial\beta}\right) = \frac{\beta}{(1-\beta^2)^{\frac{3}{2}}}$$

As a last step:

$$\left(\frac{\partial\beta}{\partial M_H}\right) = 2E_\tau c p_{\tau,x} \left[\frac{-24E_\tau^2 cp_{\tau,x}^2 M_H^8 + 4E_\tau^2 M_H^6 \left(M_H^2 + M_{\tau+}^2\right)^2 + 4cp_{\tau,x}^2 M_H^4 \left(M_H^2 + M_{\tau+}^2\right)^3 + 24E_\tau^2 M_{\tau+}^4 cp_{\tau,x}^2 M_H^4 - 2E_\tau^2 M_H^4 \left(M_H^2 + M_{\tau+}^2\right)^3 - M_H^4 \left(M_H^2 + M_{\tau+}^2\right)^4}{M_H \left(4cp_{\tau,x}^2 M_H^2 + \left(M_H^2 + M_{\tau+}^2\right)^2\right)^2 \sqrt{16E_\tau^2 cp_{\tau,x}^2 M_H^4 - 4E_\tau^2 M_H^2 \left(M_H^2 + M_{\tau+}^2\right)^2 + \left(M_H^2 + M_{\tau+}^2\right)^4}} + \right.$$

$$\left. + \frac{2E_\tau^2 M_{\tau+}^2 M_H^2 \left(M_H^2 + M_{\tau+}^2\right)^3 + M_H^2 \left(M_H^2 + M_{\tau+}^2\right)^5 - 4E_\tau^2 M_{\tau+}^4 M_H^2 \left(M_H^2 + M_{\tau+}^2\right)^2 - 4M_{\tau+}^2 cp_{\tau,x}^2 M_H^2 \left(M_H^2 + M_{\tau+}^2\right)^3 + M_{\tau+}^4 \left(M_H^2 + M_{\tau+}^2\right)^4 - M_{\tau+}^2 \left(M_H^2 + M_{\tau+}^2\right)^5}{M_H \left(4cp_{\tau,x}^2 M_H^2 + \left(M_H^2 + M_{\tau+}^2\right)^2\right)^2 \sqrt{16E_\tau^2 cp_{\tau,x}^2 M_H^4 - 4E_\tau^2 M_H^2 \left(M_H^2 + M_{\tau+}^2\right)^2 + \left(M_H^2 + M_{\tau+}^2\right)^4}} \right]$$

References

[1] G. Aad, et al. "Observation of a new particle in the search for the Standard Model Higgs boson with the ATLAS detector at the LHC." *Physics Letters B 716.1* .2012. pp. 1-29. [arXiv:1207.7214]

[2] S. Chatrchyan, et al. "Observation of a new boson at a mass of 125 GeV with the CMS experiment at the LHC." *Physics Letters B 716.1.* 2012. pp. 30-61. [arXiv:1207.7235]

[3] G. Castelo Branco, et al. "Theory and phenomenology of two-Higgs-doublet models." *Physics reports 516.1-2* .2012. pp. 1-102. [arXiv:1106.0034]

[4] J. F. Gunion, et al. *The Higgs Hunter's Guide*. Frontiers in Physics, 80. Westview Press. 2000. ISBN: 978-0738203058

[5] V. Keus ; S. F. King; S. Moretti. "Three-Higgs-doublet models: symmetries, potentials and Higgs boson masses". *Journal of High Energy Physics*, 2014, vol. 2014, no 1, pp. 1-55.

[6] J. Gradin. "Searching for a charged Higgs boson and development of a hardware track trigger with the ATLAS experiment" *Uppsala Universitet thesis*. 2017.http://uu.diva-portal.org/smash/get/diva2:1139995/FULLTEXT01.pdf

[7] Akeroyd, A. G., et al. "Prospects for charged Higgs searches at the LHC". *The European* , 17, vol. 77, no 5, pp. 1-33. [arXiv:1607.01320]

[8] D. E. Soper. "Parton distribution functions". *Nuclear Physics B-Proceedings Supplements*, 1997, vol. 53, no 1-3, pp. 69-80. [arXiv:9609018]

[9] R. D. Ball, et al. "Parton distributions from high-precision collider data." *The European Physical Journal C*, 2017, vol. 77, no 10, pp. 1-75. [arXiv:1706.00428]

[10] ATLAS. "First combination of Tevatron and LHC measurements of the top-quark mass". *arXiv preprint.*, 2014. [arXiv:1403.4427]

[11] Vector Boson Fusion. CERN. (accessed 2022, November 7) https://atlas.cern/glossary/vector-boson-fusion

[12] A. Sopczak "Cross-sections and branching ratios for charged Higgs searches". *arXiv preprint*, 2009. [arXiv:0907.1498]

[13] J. F. Donoghue, L. Fong Li. "Properties of Charged Higgs Bosons". *Phys.Rev.D 19* .1979. [doi.org/10.1103/PhysRevD.19.945]

[14] R.V. Harlander; S. Liebler; H. Mantler. "SusHi: A program for the calculation of Higgs production in gluon fusion and bottom-quark annihilation in the Standard Model and the MSSM". *Computer Physics Communications*, 2013, vol. 184, no 6, pp. 1605-1617. [arXiv:1212.3249]

[15] B. Burghgrave. "Search for Charged Higgs Bosons in the tau + LEPTON Final State With 36.1 fb–1 of pp Collision Data Recorded at s = 13 Tev With the ATLAS Experiment." .2018. *Graduate Research Theses & Dissertations*. 4836. http://pqdtopen.proquest.com/#viewpdf?dispub=10839888.

[16] N. Bakhet; M. Yu Khlopov; T. Hussein. "Neural networks search for charged Higgs boson of two doublet Higgs model at the hadrons colliders". *arXiv preprint.* 2015 [arXiv:1507.06547]

[17] J. Wenninger, M. Hostettler. "LHC Report: colliding at an angle". Accelerators. 2017. https://home.cern/news/news/accelerators/lhc-report-colliding-angle

[18] G. Aad, et al. "Evidence for the spin-0 nature of the Higgs boson using ATLAS data". *Physics Letters B*, 2013, vol. 726, no 1-3, pp. 120-144. [arXiv:1307.1432]

[19] D. Griffiths. *Introduction to Elementary Particles*. 2nd Edition. Wiley. 2008. ISBN: 978-3-527-40601-2

[20] J. William Rohlf, *Modern Physics from a to Z0*, Wiley, 1994. sec.4-4. ISBN: 9780471572701.

[21] "Life of the Higgs boson".CMS Collaboration. (accessed 2022, November 11)https://cms.cern/news/life-higgs-boson

[22] A. Albert. "Les Houches Event Files reader".(accessed 2022, November 11) https://pypi.org/project/lhereader/

[23] F. Krauss, et al. "Monte Carlo Particle Numbering Scheme". *Particle Data Group.* 2019. https://pdg.lbl.gov/2020/reviews/rpp2020-rev-monte-carlo-numbering.pdf

[24] J. Aalwall, et al. "The automated computation of tree-level and next-to-leading order differential cross sections, and their matching to parton shower simulations". *Journal of High Energy Physics*, 2014, vol. 2014, no 7, p. 1-157. [arXiv:1405.0301]

[25] Alwall, Johan, et al. MadGraph 5: going beyond. Journal of High Energy Physics, 2011, vol. 2011, no 6, pp. 1-40. [arXiv:1106.0522]

[26] F. Maltoni; T. Stelzer. "MadEvent: Automatic event generation with MadGraph". *Journal of High Energy Physics*, 2003, vol. 2003, no 02, pp. 027. [arXiv:hep-ph/0208156]

[27] LHE file to analyse. [Link]

[28] Personal files of the project "Charged Higgs Bosons at the LHC". [Link]

[29] Pedrotti and Pedrotti . *Introduction to Optics*. Prentice Hall. 1993. ISBN 0135015456.

[30] Paolo Azzurri. "The CMS Silicon Strip Tracker". *Journal of Physics: Conference Series 41* .2006. pp. 127–134. https://cds.cern.ch/record/914891/files/jpconf6_41_011.pdf

[31] M. Hashe. "Light Charged Higgs discovery potential of CMS in $H^{\pm} \to \tau\nu$ and $H^{\pm} \to W^{\pm}h^0$ ".A Thesis presented to The Academic Faculty. [hep-ph/894085]

[32] Spiropulu, Maria; Steinar, Stapnes. "LHC's ATLAS and CMS detectors." *International Journal of Modern Physics A*. 2008. 23:25, 4081-4105 https://indico.cern.ch/event/17914/contributions/299473/attachments/236169/330630/atlas-cms-final.pdf

[33] "ATLAS delivers new direct measurement of the top-quark decay width with improved precision." *ATLAS Collaboration*. 2019. (accessed 2022, November 17) https://atlas.cern/updates/briefing/direct-measurement-top-width#:~:text=Decays%20resulting%20from%20new%20physics,quark%20mass%20of%20172.5%20GeV.